Computational study of the contraction and friction mechanisms in a part manufactured by injection overmolding

Jorge Manuel Ferreira Mota Bernardino

jorge.bernardino@ist.utl.pt

Instituto Superior Técnico, Universidade de Lisboa, Portugal

June 2019

Abstract

Nowadays specialized computational software allows the simulation of the creation of complex parts by injection overmolding, where in the end of the process the polymer may have anisotropic properties that result from fiber reinforcements. In order to analyze the behavior of this type of parts, it is necessary to have the ability to pass information about the overmolding process from specialized injection software, such as Moldflow, to software that allows the structural analysis of the part, such as Abaqus, considering the interactions that exist between the components of the overmolded part. In order to pass the information regarding the anisotropy of the polymer material, a multiscale integration software, such as Helius PFA, will be used. Having done the study of the methodology regarding passing the required information and obtaining the files that allow the structural analysis to be carried out with all the parameters under consideration, it will be verified the effect that the contraction and friction phenomena have not only on the residual deformations resulting from the overmolding process as well as in the response of the part to external requests.

Keywords: Contraction, friction, tensile force, bending moment, injection overmolding

1 Introduction

To create a part with complex properties obtained from conjugating different types of materials, it is very important to understand what happens in the contact interface between the different components of the part. More complex methods are sought after, and regarding polymeric materials one solution is the application of injection overmolding.

To properly analyse an overmolded part, it is necessary to be able to account the anisotropic information when the polymeric material is reinforced by short fibers, and such properties need to be transposed to the structural analysis. Specialized software is

available to perform each specific step of this process, such as Moldflow [1] for the injection overmolding simulation, and Helius PFA [2] to perform the mapping of injection results to the structural analysis files.

It is also very important to understand the phenomena that occur in the contact interface between the components, therefore the effect of friction and polymeric contraction will be the focus point of this thesis.

2 Injection overmolding

Injection overmolding is a subcategory of multimaterial injection molding [3], which englobes all types of this kind of injection operation where multiple materials are linked together.

The cyclic operational process, especially with the usage of metal inserts, is very similar to the regular injection operation, whose different stages are:

1. Insert allocation and mold closing
2. Filling – The molten material will be injected into the mold;
3. Packing – The control is made by constant pressure, allowing the addition of material to negate contraction effects as cooling starts;
4. Cooling – The circulation of refrigeration liquid in the mold allows the molten material to cool faster until it is ready to be ejected from inside the mold with the insert connected, constituting a sole part.
5. Ejection – The mold opens and the part is ejected, allowing the cycle to begin again.

2.1 Material compatibility

A key aspect regarding the success of multimaterial injection molding processes is the compatibility of the materials that are being combined, where it is necessary to consider some parameters such as [4]:

- Thickness effects – uniform thickness leads to uniform pressure distribution;
- Melting temperature – the overmolded material should have lower melting temperature than the insert.
- Friction between surfaces – correlated with rugosity, establishes shear behaviour;
- Chemical adhesion – enhances the material connection;
- Chemical properties – One material shouldn’t cause negative effects on the others, such as corrosion;
- Mechanical interlock – Reinforces the structural stiffness of the connection.

2.2 Warpage

The cooling stage of the process causes shrinkage in the polymeric part, resulting in warpage caused by residual stresses. This deformation is causes by various phenomena that occur during the different phases of the process, ending up affecting the part properties after reaching an equilibrium state. The different types of residual stresses are [5]:

- Flow induced residual stresses – Result from the molecular orientation caused by the injection process;
- Thermal-induced stresses – Result from the progressive cooling across the thickness, which is not uniform due to

the fact the material cools faster the closest it is to the mold surfaces.

While the material is still restricted by the mold surfaces, the accumulated stresses are denominated as in-cavity stresses. After the ejection of the part, these stresses will change until the part reaches equilibrium. Due to limitations in computational calculations, Moldflow considers the part to always be restricted by the mold so it has boundary conditions to perform the calculations, therefore the data obtained is related to the in-cavity stresses and deformation.

3. Moldflow – Injection overmolding simulation

The part studied in this project is presented in Figure 1. It is composed by a polymeric component with four through holes, one circular non-through hole and a slit where the insert will be positioned.

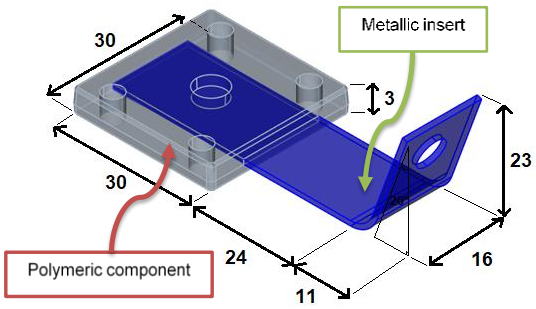

Figure 1 - Part studied in this project

The part will be created in Solidworks, as well as a 3D fan gate that will also be used. This fan gate will be one of the two different runner systems used, the other being a full hot runner system, with the latter being the one analysed the most.

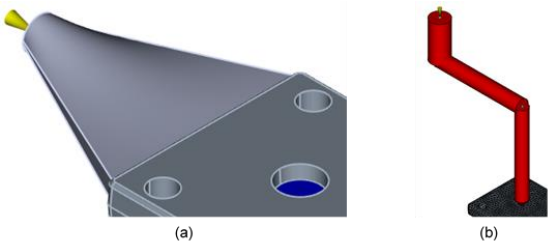

Figure 2 - Runner systems used for this part

It is now possible to create a mesh, which will initially use Dual-Domain elements for correction purposes. After that, it will be converted to 3D. The mesh used has 101796 tetrahedral elements with 1.4mm of global dimension.

The polymeric material used is a polypropylene reinforced with glass fiber in 40% of the volume, denominated GF477HP. The metallic insert will be the high strength low alloy steel HX 260LAD.

3.1 Fill+pack+warp

A fill+pack+warp analysis was performed for each runner system with the main process settings being displayed in Table 1.

Table 1 - Process setting used in F+P+W analysis

Property	Value
Mold surface temperature (C)	40
Melt temperature (C)	240
Insert initial temperature (C)	40
Injection time (s)	0.8
Cooling time (s)	20

This leads to different warpage results in both cases. With the injection overmolding analysis completed, it is now needed the ability to transpose data regarding fiber orientation and residual stresses from these analysis to the structural software.

4. Helius PFA

Helius PFA is a software that allows the transposition of the results from the relevant injection analysis variables to a structural analysis software, using Advanced Material Exchange (AME) as a data mapping tool between injection and structural meshes [2].

The multiscale model used by AME assumes that reinforcing fibers do not exhibit any behaviour in the plastic or rupture regime, having only linear elastic behaviour, while the matrix shows behaviour in both plastic and rupture regime [2];

4.1 Homogenization - decomposition cycle of the material

For the structural simulation programs to be able to simulate the behavior of the fiber reinforced composite, and considering the inability of these programs to consider the loading behavior of a material with the properties of the matrix and separate fibers, it is necessary to resort to a method which constructs a homogenized material, i.e., has no differentiation between fibers and matrix, but behaves equivalent to the reinforced composite material concerned.

The constitutive properties of the matrix and the fibers are introduced in the Mori-Tanaka incremental micromechanical model [6] that can accommodate the evolutionary matrix properties. This micromechanical model produces the homogenized properties of the idealized composite with perfect fiber alignment. These properties are in turn operated by the fiber orientation tensor, producing the homogenized properties of the actual material with the already oriented fibers.

In order to simulate the behaviour of the material in rupture state it is necessary to decompose the extension of the homogenized material into the average extension of the matrix.

The decomposition process begins by reversing the homogenization process, taking in the extension values obtained during the increment of the structural analysis. It then uses the Mori-Tanaka incremental micromechanical model, the instant constituent properties and the orientation tensor of the fibers in order to decompose this increment and calculate the average extension in the matrix that is used to guide the matrix plasticity and rupture model to their behaviour. The homogenization - decomposition cycle is repeated until the end of the analysis.

4.3 Plasticity model

Helius PFA uses a modified Ramberg-Osgood plasticity criterion [7] in order to obtain the behaviour of the constituent matrix of the material with the ability to predict the plastic response sensitive to the direction of loading performed with respect to the orientation of the fibers [2]. This is done by adding additional coefficients to the equations of the model regarding various parameters such as effective strain.

4.4 AME stages

After importing the injection and structural files, obtained from Moldflow and Abaqus [8] respectively, the imported geometries must be aligned in order to map the variables in the way that is wanted.

it is now necessary to choose the material model, which in this case was chosen

the Elastic-Plastic model, so that the non-linear behaviour of the material can be considered.

Since the Elastic-Plastic model was selected, it is now required to import the stress-strain data of the material according to three different fiber orientations, those being 0º, 90º and 45º (optional), in tensile or compressive regime if required.

In order to properly map the variables in the structural mesh, it is necessary to verify the compatibility between meshes. This is possible using the Mapping Suitability Plot tool. If the results are not satisfactory, both meshes should be refined in order to obtain proper compatibility results, which influence the accuracy of further structural analysis.

Finally, it is now possible to map the results from the injection process in the structural mesh, allowing to export the final files with all the information needed for the structural analysis. In Figure 3 the mapped fiber orientation tensor in the structural mesh of case *hot runner sim* is displayed.

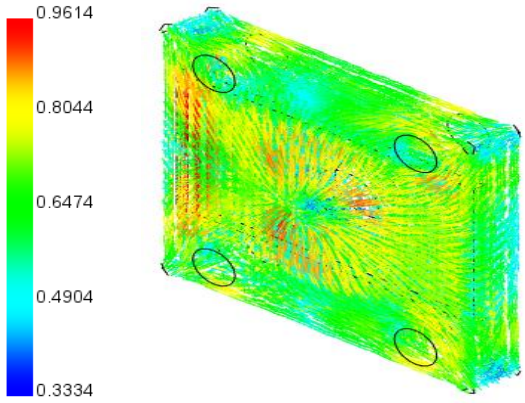

Figure 3 – Fibers mapped in the structural mesh (hot runner)

5. Structural analysis - Abaqus

The workflow used in this project in order to obtain the files required to perform the structural analysis of the part in displayed in Figure 4.

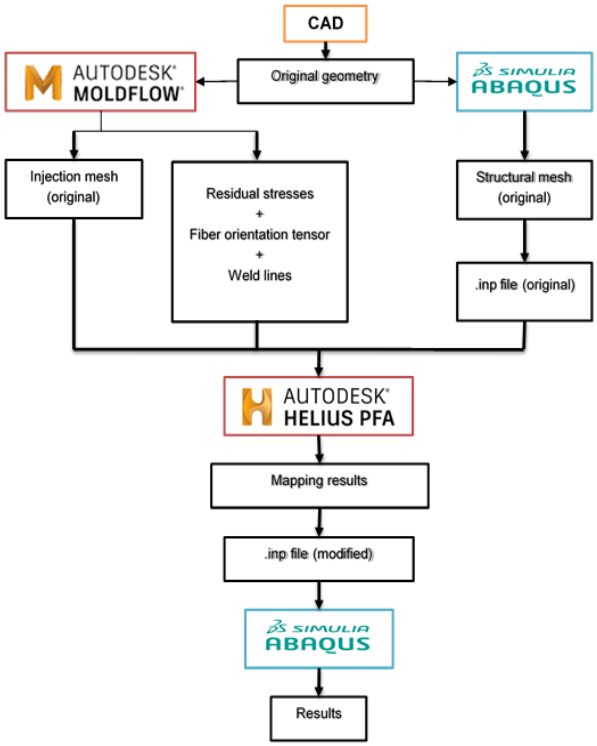

Figure 4 - Project workflow

5.1 Structural mesh

Another mesh was created in Abaqus which corresponds to the final mesh that will perform the structural deformation (Figure 5). It also used tetrahedral elements, these being quadratic (C3D10).

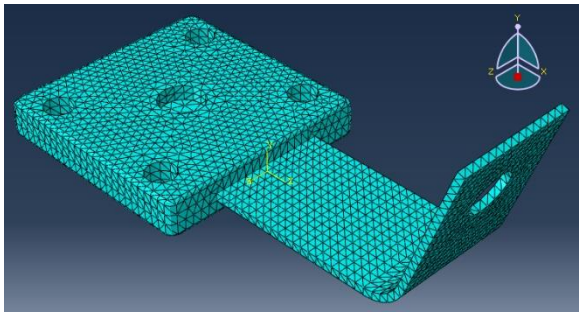

Figure 5 - Structural mesh

5.2 Step definition

The steps that were created and characterized are the following:

- Initial step – where the contact parameters will be defined;
- Step-0, where the energy stabilization method will be applied, in order to simulate the warping of the part resulted from the residual stresses;
- Step-Forces – where the loads and boundary conditions are applied.

5.3 Contact definitions

In order to evaluate the friction influence in the deformation results, it was chosen in Abaqus the global contact interaction method, which allows the consideration of every single possible surface interaction, as well as corners. It will also correct the initial position of the surface nodes to avoid clearance or overclosure [8].

5.4 Energy stabilization method

In order to obtain the warpage predicted by Moldflow it is necessary to solve a non-linear problem where there are no loads, rigid body movements and boundary conditions applied.

One of the methods available in Abaqus to solve this type of problem is the energy stability method [8].

A term corresponding to the viscous forces F_v is considered, being it:

$$F_v = c * M * v \qquad (5.1)$$

where c is the damping coefficient, M is an artificial mass matrix calculated with unit density and v is the vector of nodal velocities. F_v corresponds to the energy dissipated during the deformation making possible the elimination of the effects of rigid body movement.

The damping coefficient is calculated based on the fraction of energy dissipated from deformation. Initially the problem is considered stable, with the viscous forces and corresponding dissipated energy being very small. The instabilities are developed along the step, causing the increase of local velocities and, consequently, dissipation of part of the energy through the applied damping. The predefined energy dissipation fraction is equal to 0.0002 [8], this being the value used in this project.

In this step, another parameter that must be considered is the friction coefficient, which will affect the results regarding the dissipated energy and thus the deformation. In Figure 6, an example of deformation in z axis is displayed for the results provided by Moldflow for the hot runner sim case (a) and the Step-0 results (b) for such case with μ = 0.4, μ being the friction coefficient.

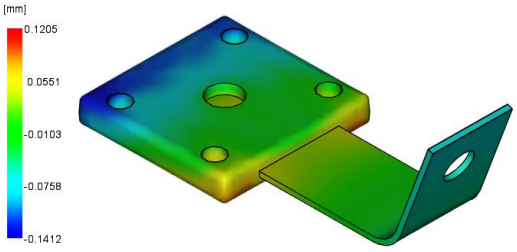

(a)

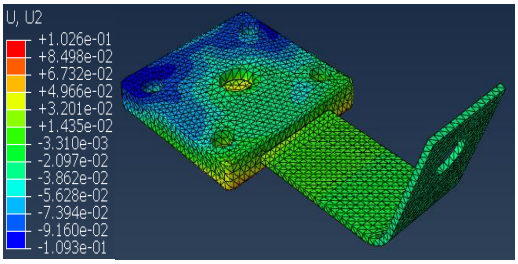

(b)

***Figure 6 – Deformation results for the z axis with* μ = 0.4: (a) Moldflow; (b) *Step-0* no Abaqus**

5.5 External Loads and boundary conditions

There will be two different types of loads applied in the part:

1) Case Tr – A tensile load will the applied in the metal insert, as it can be seen in Figure 7. It will allow the study of frictional behaviour in the contact surfaces without interference from other types of phenomena;

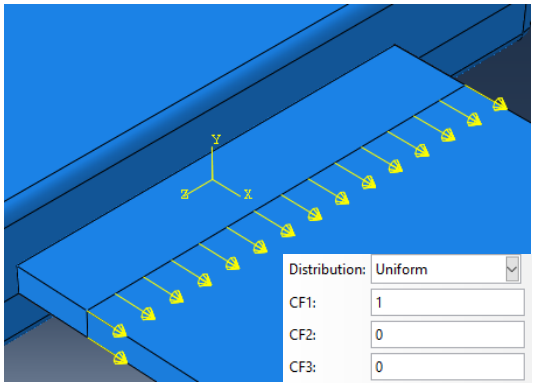

Figure 7 – Tensile force applied

2) Case Nor – A bending load will be applied in the hole of the insert (see Figure 8) in order to analyse the influence of bending in the friction phenomena.

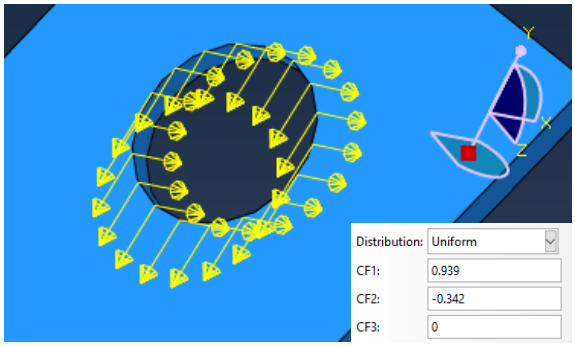

Figure 8 – Normal force applied

The boundary conditions will only be applied in Step-Forces, establishing that the through holes will verify a pinned constraint, as it can be seen in Figure 9.

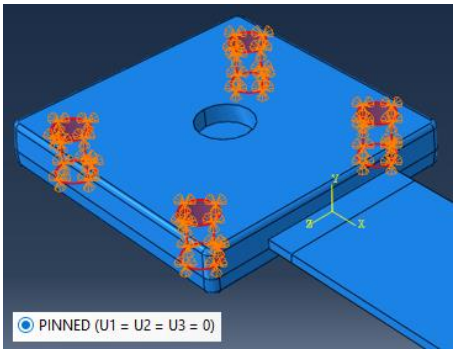

Figure 9 – Established boundary conditions

After this being defined, it is now possible to integrate the Moldflow results in the structural mesh using Helius PFA.

6. Results and discussion

6.1 Step-0

As it is shown in Figure 10, in general the energy plots increase until reaching approximately μ = 0.4.

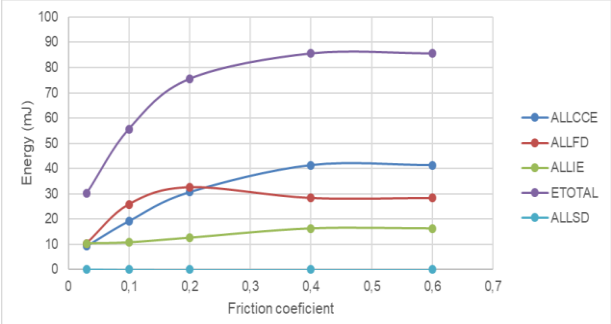

Figure 10 – Evolution of the energy plots with the coefficient of friction variation (Step-0)

ALLCCE is the contact constraint elastic energy, ALLFD is the energy dissipated through frictional effects, ALLIE is total strain energy, ALLSD is the energy dissipated by

automatic stabilization and ETOTAL is the total energy balance, which represents the sum of all other energy plots:

$$ETOTAL = ALLCCE + ALLFD + ALLIE + ALLSD \quad (6.1)$$

The higher the friction coefficient the greater are the areas where there is closed contact (no relative displacement between surfaces) as well as slip zones, as can be seen in Figure 11.

Therefore, it is understood that it is necessary to provide more energy to the part so that it can deform, due to the resistance imposed by the contact, hence the increase of the ALLIE plot.

As the contact area increases, the elastic energy will also increase since there will be more energy stored elastically in these areas, ready to be released when separation occurs.

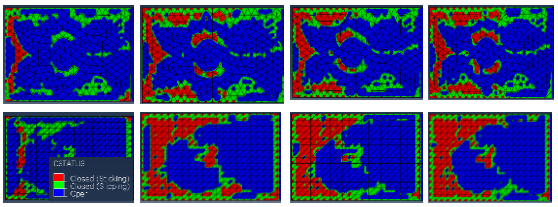

(a) (b) (c) (d)

Figure 8 – Contact status in both sides of the insert for: (a) μ = 0,03; (b) μ = 0.2; (c) μ = 0.4; (d) μ = 0.6

As it happens in the variation of the energy involved in the process of residual deformations, these deformations are approaching the values obtained in Moldflow as the friction coefficient grows, verifying a negligible difference in the values relative to the deformations, particularly the maximum value, corresponding to the friction coefficients equal to 0.4 and 0.6.

Table 2 - Magnitude of the deformation regarding different friction coefficients

μ	Umag		Aprox. Umag (%)	
	máx	**min**	**máx**	**min**
0.03	0.225	0.0016	19.51	43.75
0.2	0.201	0.0024	9.86	62.50
0.4	0.186	0.0011	2.42	18.18
0.6	0.178	0.0012	1.51	25.00
Moldflow	0.181	0.0009	-	-

In order to clearly visualize the contact interface, the displacement variation and the tension state, a section of the deformed part resulted from the shrinkage of the polymer is shown in Figure 12, with the deformation being visually amplified by a factor of 10, according to an xy plane located at half thickness by the end of Step-0. The polymeric shrinkage promoted the creation of a gap between surfaces located in the bottom section near the slit's opening, while it pushes the insert towards the hole. Meanwhile, near the slit's end, the insert remains locked in place.

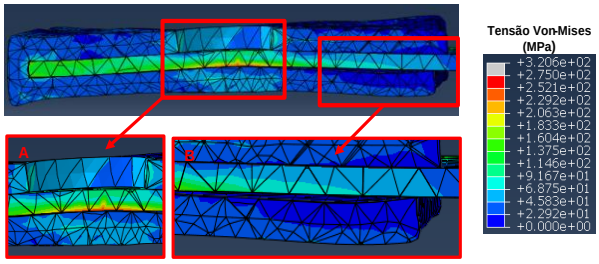

Figure 12 – von Mises stresses in a cut section by the xy plane at half thickness (Step-0)

6.2 Case Tr

6.2.1 Rupture

The variation of SDV1 (variable provided by Helius PFA to check the rupture state) indicates that the friction phenomena do not condition the force corresponding to the initialization of rupture (SDV1 > 1) regarding the composite material, being this an essential parameter to evaluate the resistance of the part

to the loads without degradation. In addition, no differences were observed in the evolution of zones affected by rupture.

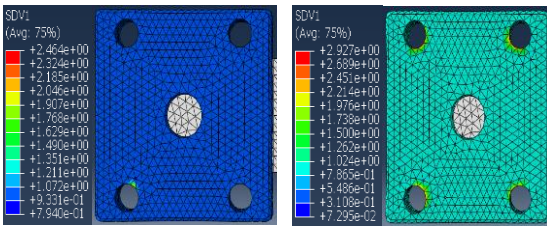

(a) (b)

Figure 9 - Propagation of regions affected by rupture (case Tr): a) t=0,716; b) t=1,216s

The rupture of the composite material starts at the increment corresponding to the instant t = 0.716 seconds, where a force of approximately 220N is applied, which means that this is the force value that defines the pure traction regime relative to breakage.

6.2.2 Friction effect on deformation

It is possible to verify that the smaller the coefficient of friction is the greater is the displacement verified in a node from a plane situated in the insert close to the slit opening, for a force of equal intensity, as it is shown in Figure 14.

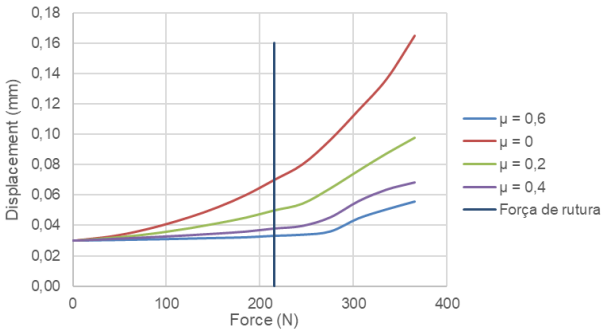

Figure 14 – Displacement – Force plot regarding various friction coefficients (case Tr)

It is important to note that the influence of the friction phenomena is visible almost immediately after the beginning of the deformation of the part due to the immediate discrepancy verified in the evolution of the curves, long before reaching the moment where the rupture begins. With the increased intensity of the friction phenomena, the necessity arises to impose a more intense force in order to obtain the same displacement, due to the resistance offered by the friction between surfaces, in addition to registering a greater number of contact areas, matching what happens in Step-0.

6.3 Case Nor

Since there is simultaneously tensile and bending in the plate, the manifestation of the effects resulting from friction allows the separation regarding the bending and tensile influence, in addition to verifying which of these components is dominant since the friction will manifest itself due to the tensile component of the force. To obtain this relation, it was observed the difference between the displacement of a point in the top with another in the bottom of the same plane that was mentioned in Case Tr, which is displayed in Figure 15.

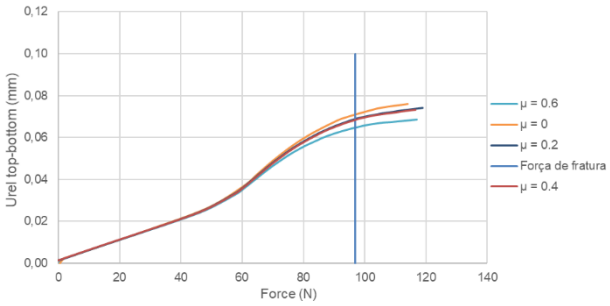

Figure 15 - Displacement – Force plot regarding various friction coefficients (case Nor)

When the friction coefficient is higher, the displacement provided by the tensile component will decrease (until stabilization of results), so the difference between total

displacements (in modulus) at these points will be smaller. It will be in this divergence of results that from the observation of Figure 15 it is understood that the friction phenomena only influence the deformation when the applied force reaches approximately the value of 75N because it is from there that the curves relative to the simulations with friction diverge from the frictionless simulation curve.

Given that rupture occurs at a very close instance, when the force reaches the 97N, it is possible to conclude that the regime that dominates the deformation of the part until the rupture point is the bending, whereas after that the tensile component allied with the friction phenomena happens to influence more preponderantly the displacements.

7. Conclusion

It was proven that the deformation caused by residual stresses is affected by the complementarity between the mechanism of shrinkage with the friction phenomena.

It was also verified that the existence of friction phenomena does not affect the rupture regime.

In addition, it was verified that when the bending regime is present, it is dominant and completely changes the deformation and the instance where the rupture and the preponderance of the friction phenomena occurs.

References

[1] Autodesk, “Moldflow - Plastic Injection Molding Design Software”. URL: https://www.autodesk.com/products/moldflow/overview [January 2019]

[2] Autodesk knowledge network – Helius PFA, “Theory Manual”. URL: https://knowledge.autodesk.com/support/helius-pfa/learn-explore/caas/CloudHelp/cloudhelp/2019/ENU/ACMPAN-AME/files/GUID-D60A05C0-DD63-47B6-B1CD-248F2BDF1A9D-htm.html

[3] “Multi-material injection molding summary”. URL: https://chemtec.org/products/978-1-85957-327-3 [February 2019]

[4] “3 Key Elements to Consider When Designing for Overmolding”. URL: https://www.protolabs.com/resources/design-tips/designing-for-overmolding/ [March 2019]

[5] “Residual Stress – A Culprit in Shrinkage and Warpage Problems”. URL: http://www.dc.engr.scu.edu/cmdoc/dg_doc/develop/process/physics/b3400001.htm [March 2019]

[6] Mori, T., Tanaka, K. (1973). Average Stress in Matrix and Average Elastic Energy of Materials With Misfitting Inclusions. ACTA METALLURGICA

[7] Ramberg, W. Osgood, W.R. (1943). Description of Stress-Strain Curves by Three Parameters. Technical Notes, National Advisory Comitee for Aeronautics.

[8] Abaqus 2017 Documentation